

The First Mammalian Aldehyde Oxidase Crystal Structure

INSIGHTS INTO SUBSTRATE SPECIFICITY*[§]

Received for publication, June 28, 2012, and in revised form, September 26, 2012. Published, JBC Papers in Press, September 27, 2012, DOI 10.1074/jbc.M112.390419

Catarina Coelho[‡], Martin Mahro[§], José Trincão[‡], Alexandra T. P. Carvalho[¶], Maria João Ramos[¶], Mineko Terao^{||}, Enrico Garattini^{||}, Silke Leimkühler[§], and Maria João Romão^{‡1}

From the [‡]Requimte, Departamento de Química, Faculdade de Ciências e Tecnologia, Universidade Nova de Lisboa, 2829-516 Caparica, Portugal, [§]Universität Potsdam, Institut für Biochemie and Biologie, 14476 Potsdam, Germany, [¶]REQUIMTE, Departamento de Química e Bioquímica, Faculdade de Ciências, Universidade do Porto, Rua do Campo Alegre s/n, 4169-007 Porto, Portugal, and the ^{||}Laboratory of Molecular Biology, Department of Biochemistry and Molecular Pharmacology, Istituto di Ricerche Farmacologiche Mario Negri, via La Masa 19, 20156 Milano, Italy

Background: Aldehyde oxidases have pharmacological relevance, and AOX3 is the major drug-metabolizing enzyme in rodents.

Results: The crystal structure of mouse AOX3 with kinetics and molecular docking studies provides insights into its enzymatic characteristics.

Conclusion: Differences in substrate and inhibitor specificities can be rationalized by comparing the AOX3 and xanthine oxidase structures.

Significance: The first aldehyde oxidase structure represents a major advance for drug design and mechanistic studies.

Aldehyde oxidases (AOXs) are homodimeric proteins belonging to the xanthine oxidase family of molybdenum-containing enzymes. Each 150-kDa monomer contains a FAD redox cofactor, two spectroscopically distinct [2Fe-2S] clusters, and a molybdenum cofactor located within the protein active site. AOXs are characterized by broad range substrate specificity, oxidizing different aldehydes and aromatic *N*-heterocycles. Despite increasing recognition of its role in the metabolism of drugs and xenobiotics, the physiological function of the protein is still largely unknown. We have crystallized and solved the crystal structure of mouse liver aldehyde oxidase 3 to 2.9 Å. This is the first mammalian AOX whose structure has been solved. The structure provides important insights into the protein active center and further evidence on the catalytic differences characterizing AOX and xanthine oxidoreductase. The mouse liver aldehyde oxidase 3 three-dimensional structure combined with kinetic, mutagenesis data, molecular docking, and molecular dynamics studies make a decisive contribution to understand the molecular basis of its rather broad substrate specificity.

Aldehyde oxidases (AOXs,² EC 1.2.3.1) are a small group of evolutionarily conserved proteins belonging to the family of

molybdo-flavoenzymes along with xanthine oxidoreductase (XOR), the key enzyme in the catabolism of purines (1–3). In their catalytically active form, molybdo-flavoenzymes function as homodimers and require a molybdenum cofactor (Moco) as well as flavin adenine dinucleotide (FAD) to oxidize their substrates. AOXs and XORs are characterized by similar primary structures (~50% amino acid identity) and are evolutionarily related enzymes (4–8). In fact, the extant complement of AOX genes evolved from an XOR ancestral precursor via a series of gene duplication and suppression/deletion events (3, 9). In the animal kingdom, AOXs are present in virtually all species from insects to humans. Different animal species contain a different complement of AOX genes encoding an equivalent number of AOX isoenzymes. In mammals, the two extremes are represented by certain rodents such as mice and rats, which are endowed with four AOX genes, and by humans, whose genome is characterized by a single active gene. In mice, the four AOX loci (*Aox1*, *Aox3*, *Aox4*, and *Aox3l1*) form a cluster and map to a small region of chromosome 1 band c1. The products of the four mouse *Aox* genes are expressed in a tissue- and organ-specific fashion (1). The mouse AOX1 and AOX3 proteins are synthesized mainly in the liver (5). The richest source of AOX4 is the Harderian gland, a major structure located in the orbital cavity (4, 10). Finally, AOX3L1 expression is restricted to the Bowman's gland of the nasal mucosa (11). In these sites, the four AOXs are hypothesized to perform undefined tissue and organ specific functions, possibly acting on a different or overlapping set of substrates (1). The only functional gene present in humans is the ortholog of mouse *Aox1* (6). The human *Aox1* gene is located on chromosome 2p near two inactive pseudogenes, representing the vestiges of the mouse *Aox3* and *Aox3l1* orthologs (6). Large amounts of AOX1 are present in the cyto-

* This work was supported by the Portuguese Science and Technology Foundation (FCT-MCTES) through Project PTDC/BIA-PRO/118377/2010 and Grant SFRH/BD/37948/2007 (to C. C.) and by the Cluster of Excellence "Unifying Concepts in Catalysis" (to S. L. and M. M.) coordinated by the Technische Universität Berlin and funded by the Deutsche Forschungsgemeinschaft. The exchange of researchers among laboratories was funded by the DAAD-GRICES program (to M. J. R. and S. L.). The work was also supported by grants from the Associazione Italiana per la Ricerca contro il Cancro (AIRC), the Fondazione Italo Monzino, and the Negri-Weizmann Foundation (to E. G.).

[§] This article contains supplemental Experimental Procedures, Results and Discussion, and Figs. S1–S3.

The atomic coordinates and structure factors (code 3ZYV) have been deposited in the Protein Data Bank (<http://www.pdb.org/>).

¹ To whom correspondence should be addressed. E-mail: maria.romao@fct.unl.pt.

² The abbreviations used are: AOX, aldehyde oxidase; mAOX3, mouse AOX3; Moco, molybdenum cofactor; XO, xanthine oxidase; XOR, xanthine oxi-

doreductase; bXOR bovine XOR; XDH, xanthine dehydrogenase; ESRF, European Synchrotron Radiation Facility; DCPIP, 2,6-dichlorophenolindophenol; NCS, non crystallography symmetry.

sol of human hepatocytes, although detectable levels of the protein are also found in many other tissues (12).

Mammalian AOXs are characterized by broad substrate specificity and metabolize a wide range of endogenous and exogenous compounds (12). They oxidize organic molecules containing an aldehyde functionality into the corresponding carboxylic acid and hydroxylate numerous types of aza- and oxo-heterocycles. Given their broad substrate specificity, human AOX1 is considered to be the major cytosolic enzyme involved in phase I metabolism and inactivation of drugs as well as other xenobiotics (13). In other model organisms used for drug metabolism studies, the same role is played by other AOX isoenzymes. In mice and rats, the main drug-metabolizing enzyme is AOX3, as this is the prevalent form of AOX present in the liver. The significance of AOXs for the clearance of xenobiotics is predicted to increase in the near future (13).

Here we report the structure of mouse AOX3, the first mammalian AOX to be crystallized. The crystallographic structure demonstrates that the catalytically active forms of mAOX3 and bXOR (14–16) have similar overall conformations, although significant structural differences are found in many functional domains, with particular reference to the substrate binding pocket and the Moco domain. Comparing the crystal structures of AOX and the related bXOR protein provided invaluable information as to the structural determinants responsible for the difference in substrate and inhibitor specificity. In addition, it shed light on possible differences in the catalytic mechanisms of the two types of enzymes. From an applied perspective, the structure of AOX1 or AOX3 will be instrumental in the generation of *in silico* methods for the prediction or validation of chemical structures acting as AOX substrates.

EXPERIMENTAL PROCEDURES

Protein Purification—mAOX3 was purified from CD1 mouse liver as well as from a heterologous expression system from *Escherichia coli* as reported previously (17). The recombinant mAOX3 was expressed as an N-terminal fusion protein with a His₆ tag. Both proteins were stored in 50 mM sodium phosphate, pH 8.0, 300 mM NaCl at -80°C until usage without loss of activity. Final protein concentration was 10 and 17.8 mg/ml for the native and recombinant samples, respectively, determined using the BCA protein quantification assay (Sigma).

Enzyme Assays—Steady state kinetics were performed at 37°C in 50 mM Tris-HCl, pH 8.0, and 1 mM EDTA using variable substrate (0–250 μM benzaldehyde, 0–50 μM phthalazine, 0–5 mM *N*1-methylnicotinamide, and 0–600 μM phenanthridine) and purified mAOX3 (50–200 nM) concentrations. As electron acceptors, 100 μM 2,6-dichlorophenolindophenol (DCPIP) or molecular oxygen (in the case of phenanthridine) were used in a final reaction volume of 500 μl . Enzyme activity was monitored at 600 nm for DCPIP and at 321 nm for phenanthridine. Inhibition studies of mAOX3 were performed using 0–2 μM menadione, 0–2 μM norharmane, 0–50 μM raloxifene, (solubilized in dimethyl sulfoxide, with final solvent concentration of 1% v/v), and 0–750 μM benzamidine (solubilized in assay buffer) under standard assay conditions with phthalazine. Specific activity was calculated using molecular extinction coefficients of 21,400 $\text{M}^{-1}\text{cm}^{-1}$ for mAOX3, 4775 $\text{M}^{-1}\text{cm}^{-1}$ for

phenanthridine and 16,100 $\text{DCPIP}^{-1}\text{cm}^{-1}$ for DCPIP (18). Kinetic parameters were obtained by nonlinear fitting of the Michaelis-Menten equation or the appropriate inhibition Equation 1 using R.build 2.12.00 (19),

$$\nu = \frac{V_{\max} \times [S]}{K_{\text{M}} \left(1 + \frac{[I]}{K_{\text{ic}}} \right) + [S] \left(1 + \frac{[I]}{K_{\text{iu}}} \right)} \quad (\text{Eq. 1})$$

where K_{ic} and K_{iu} are the competitive and uncompetitive inhibition constants respectively.

Crystallization—The mAOX3 protein was preincubated with 10 mM dithiothreitol for 1 h at 4°C , and crystals with approximate dimensions $0.40 \times 0.15 \times 0.05 \text{ mm}^3$ were reproducibly obtained at 20°C within 3 days using 12–16% polyethylene glycol 8000, 0.1 M potassium phosphate, pH 6.5, and 2 mM EDTA. Further details on protein crystallization were previously reported (17). The crystals were flash-cooled in liquid nitrogen using Paratone oil as cryoprotectant before transfer to a nitrogen stream. The majority of the crystals diffracted to poor resolution ($\sim 6 \text{ \AA}$) at beamline ID14-1 of the European Synchrotron Radiation Facility (ESRF, Grenoble, France), but for some of the crystals, diffraction could be improved to a resolution beyond 3 \AA using the beamline automatic annealing procedure.

Data Collection and Processing—An 180° data set of a native mAOX3 crystal was collected at ID 14-1 (ESRF) at an 0.934 \AA wavelength. The crystal belongs to space group P1, with unit cell dimensions $a = 90.9 \text{ \AA}$, $b = 135.3 \text{ \AA}$, $c = 147.4 \text{ \AA}$, and $\alpha = 78.2^{\circ}$, $\beta = 77.7^{\circ}$, $\gamma = 89.9^{\circ}$ and two dimers in the unit cell (see Table 1). All data were processed using iMosflm 1.0.4 (20) or XDS (21) to 2.9 \AA .

When processing the data with iMosflm, the mosaicity value became too unstable, probably due to crystal anisotropy, until the program crashed. The data were then processed with fixed values of mosaicity ranging from 0.3 to 1.5 in 0.1 increments. The dataset with the best overall statistics was the one with a mosaicity value of 1, which was the one used for refinement. We also processed the data with XDS, which gave a mosaicity value of 0.349. However, the electron density maps were clearly better when using data processed with iMosflm. Because the data were very anisotropic, some data were not usable due to spot overlapping, and some images had to be discarded. This explains why the final data set is only 89.8% complete (77.3% in the highest shell).

Structure Solution and Refinement—The structure was solved by molecular replacement with Phaser 2.1.4 (22) using the structure of bovine xanthine dehydrogenase (PDB ID 3bdj) as a search model after omitting all the cofactors and solvent molecules. Although the initial density was very poor, clear positive density could be observed at the expected position of the Moco, the FAD, and the two FeS cofactors, indicating the correctness of the solution. Four monomers were found in the unit cell. Density modification with 4-fold non-crystallographic symmetry averaging was performed using DM (CCP4) (23). The resulting electron density improved dramatically, allowing rebuilding one chain and applying NCS operators to transform it to the three other chains. Because the data were of relatively

The First Crystal Structure of Mouse Liver Aldehyde Oxidase

TABLE 1

Data collection, structure refinement, and model building statistics

Values in parenthesis correspond to the highest resolution shell. $R_{\text{work}} = \sum |F_{\text{calc}}| - |F_{\text{obs}}| / \sum |F_{\text{obs}}| \times 100$, where F_{calc} and F_{obs} are the calculated and observed structure factor amplitudes, respectively. R_{free} was calculated for 5% of the reflections randomly chosen for each data set. AU, asymmetric unit.

Crystal sample	mAOX3
Beamline (ESRF)	ID14-1
Wavelength (Å)	0.934
Unit cell parameters (Å, °)	$a = 90.9, b = 135.3, c = 147.4$ $\alpha = 78.2, \beta = 77.7, \gamma = 89.9$
Space group	P1
Number of molecules in the AU	4
Matthews coefficient (Å ³ /Da)	3.23
Solvent content (%)	61.5
Resolution limits (Å)	49.9–2.9
No. of observations	219,268 (20,892)
No. of unique observations	133,319 (16,784)
Multiplicity	1.6 (1.2)
Completeness (%)	89.8 (77.3)
R_{pim} (%)	5.6 (13.9)
R_{sym} (%)	5.7 (33.8)
$I/\sigma(I)$	9.6 (3.6)
CC _{1/2} outer shell (no. pairs) (24)	0.911 ($n = 1214$ pairs)
R_{free} (%)	27.02
R_{factor} (%)	24.37
Number of water molecules	654
Average B factor for all atoms (Å ²)	42.7
Root mean square deviation from ideal geometry	
Bond lengths (Å)	0.013
Bond angles (°)	1.21

low quality, NCS restraints were maintained throughout the refinement. The reported resolution of the data is 2.9 Å. The correlation coefficient between half data sets (24) for 2.9 Å resolution is $CC_{1/2} = 0.911$ (number of pairs = 1214). Initial rounds of refinement were carried out in Refmac 5.5 (22), omitting all the cofactors. After several rounds of rebuilding and refining in Coot (25), the R/R_{free} leveled off at about 26/33%. Switching to Phenix.refine (26) lowered the R_{free} to ~30%. All the following steps were carried out in Phenix, with TLS refinement (eight TLS groups per monomer) and NCS restraints with automatic weighting. In the final stages of refinement, >250 residues (~5%) would keep moving out of the Ramachandran most favored conformations. Ramachandran restraints were also added to the refinement protocol. Waters were automatically added by Phenix.refine and manually inspected in Coot. The final model contains four chains (A–D) and residues Ser-7 to Val-1334, with all the cofactors present. Some loops located at the surface, linker I (Pro-169–Thr-199; Glu-227–Asn-231), FAD domain (Gly-399–Ile-404), linker II (Asp-538–Ile-545; Leu-558–Gly-563), and Moco domain (Arg-1290–Trp-1296; Gln-1321–Pro-1329) had no visible electron density and were omitted from the model. The deposited model contains 5018 protein residues, 654 water molecules, and one sodium ion per monomer (see Table 1 for structure refinement and model statistics). The residues with disordered side chains were stubbed at $C\beta$.

RESULTS AND DISCUSSION

Overall Structure—The overall topology of mouse AOX3 and mammalian XORs are similar. In the homodimer each monomer comprises 1335 residues and can be divided into three major domains involved in binding to the cofactors (Fig. 1A). The small N-terminal domain (domain I: 20 kDa, Met-1–Pro-

169) harbors the two FeS clusters and connects to the FAD binding domain II (40 kDa, Thr-232–Leu-534) through a poorly conserved linker I region (Ser-170–Asn-231). The C-terminal and largest domain III (90 kDa, Leu-576–Ala-1335) contains the Moco binding site, with the molybdenum catalytic center located at the bottom of an ~15 Å-deep and -wide pocket. The protein cofactor disposition is consistent with the expected electron transfer pathway; electrons released from the hydroxylation reaction at the molybdenum catalytic center are transferred to the two FeS clusters and the FAD redox cofactor in sequence (Fig. 1B). Subsequently, electrons reach the final acceptor, which is exclusively O₂ in the case of AOXs.

Iron/Sulfur Domain—The two iron-sulfur clusters are located in domain I and are designated FeSI and FeSII according to their distinct EPR signals. Domain I can be further divided into two subdomains: the N-terminal sub-domain with [2Fe-2S] II (Met-1–Val-92) and the second subdomain (Glu-93–Pro-169), which binds [2Fe-2S] I. The iron saturation of the purified protein from mouse liver was determined to be 53% (17). However, the two [2Fe-2S] clusters were clearly visible in the initial electron density maps and were refined with full occupancy (Fig. 2). All the atoms in the two clusters present B factor values within the range of their surrounding atoms. This shows that only the active portion of the protein with a full occupancy of the FeS clusters has crystallized.

FAD Domain—The FAD domain can be divided into two subdomains comprising residues Thr-232–Ser-419 and Ser-420–Leu-534. The FAD cofactor is mainly coordinated by the first subdomain with residues Pro-263, Leu-264, Asn-268, Thr-269, Tyr-270, Ser-354, and Leu-411 establishing hydrogen bonds with the dinucleotide and residues His-358 and the Asp-367 contacting the riboflavin (Fig. 3). The isoalloxazine ring is stacked between two hydrophobic side chains: Leu-344 (Phe in XOR) and Phe-438 (Ile in XOR), the latter laying approximately parallel.

Moco Domain—The C-terminal domain III contains the Moco binding site, which is located at the bottom of a wide groove, leading to the catalytic center. As in related enzymes, domain III can be structurally divided into four subdomains that include non-continuous stretches of the polypeptide chain: subdomain III.1 (Leu-576–Pro-698 and Glu-745–Gly-843), subdomain III.2 (Met-699–Gln-744 and Arg-844–Phe-964), subdomain III.3, (Asp-965–Lys-1009 and Phe-1160–Val-1334), and subdomain III.4 (Phe-1010–Val-1159). All these subdomains share a similar fold, and whereas subdomains III.2 and III.3 are exposed to the solvent, subdomains III.1 and III.4 are involved in dimerization contacts.

Comparison with Structurally Related Proteins—Crystal structures from several members of the molybdo-flavoenzyme family have been reported in the past few years. The first structure reported was the *Desulfovibrio gigas* aldehyde oxidoreductase at a resolution of 2.25 Å (later refined to 1.28 Å) (27, 28). Although mAOX3 and *D. gigas* aldehyde oxidoreductase share low sequence identity (23%), their overall fold is very similar. *D. gigas* aldehyde oxidoreductase lacks the FAD domain, but its global structure superimposes to mAOX3 domains I and III (root mean square deviation of 1.83 Å for 614 C_α atoms). The crystal structure of xanthine dehydrogenase (XDH) isolated

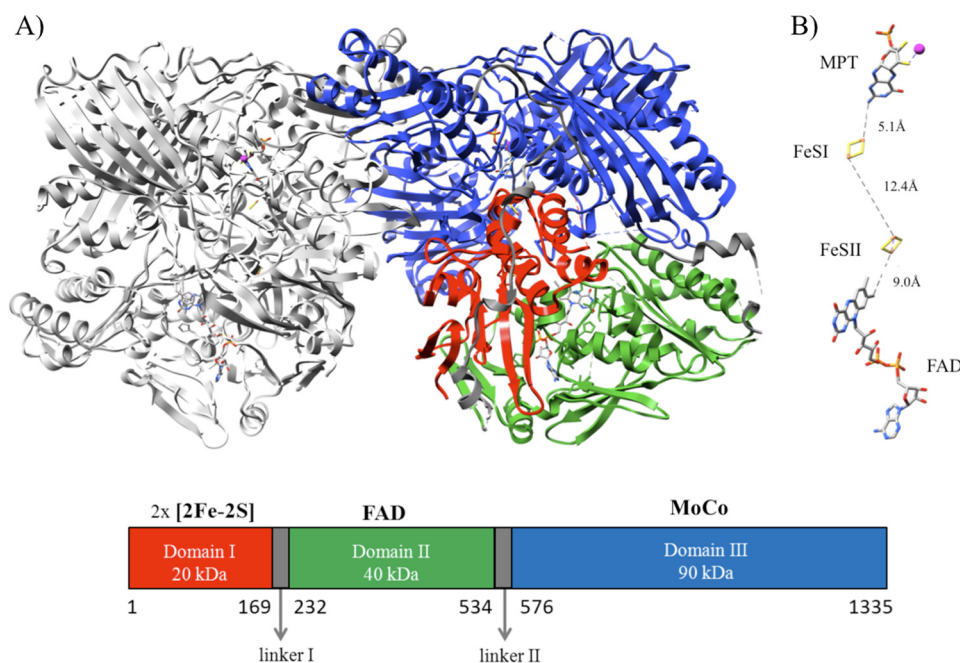


FIGURE 1. *A*, shown is a ribbon representation of the mAOX3 crystal structure. The left monomer is in *gray*. The *right monomer* is shown with the three different domains colored as follows: domain I in *red* (residues Met-1–Pro-169), domain II in *green* (residues Thr-232–Leu-534), and domain III in *blue* (residues Leu-576–Val-1335). Domain III is separated from the FAD domain by a linker II region (Lys-535–Pro-575). The linker regions are represented in *dark gray* (linker I Ser-170–Asn-231). The two mouse AOX3 monomers are tightly bound, with the majority of contacts established by residues present in the domain containing the Moco binding site. The molybdenum atoms from the two monomers are more than 50 Å apart, and most likely, the two subunits work independently as shown previously for the *R. capsulatus* xanthine dehydrogenase (51). Homodimer approximate dimensions are 150 × 90 × 70 Å. *B*, arrangement and distances between the different protein cofactors are shown. *MPT*, the two distinct [2Fe-2S] centers and FAD.

from the purple bacterium *Rhodobacter capsulatus* was published later at 2.7 Å resolution (29). Unlike mAOX3, which is a homodimer, *R. capsulatus* XDH is a homotetramer ($\alpha\beta$)₂. The two FeS clusters and the FAD are bound to the XdhA subunit, and Moco is in the XdhB subunit. Despite a different subunit composition, the overall fold and the arrangement of the cofactors are similar in mAOX3 and *R. capsulatus* XDH, and the two structures superimpose with a root mean square deviation of 1.09 Å for 913 C_α atoms. The main difference between the two proteins is the absence of the linker II region (Lys-535–Pro-575 in mAOX3) in the bacterial enzyme. The crystal structures of the bovine milk dehydrogenase (XDH) and oxidase (XO) forms of XOR were initially reported at a resolution of 2.1 and 2.5 Å, respectively (15) and later at higher resolution (1.65 Å (30)). The protein is synthesized in the dehydrogenase form but can be readily converted into the oxidase form by oxidation of sulfhydryl residues (a reversible process) or by proteolysis (irreversible) (15, 31, 32). The main difference between the two protein forms is the binding of NAD⁺, which occurs only in the XDH form. mAOX3 and bXOR are characterized by a similar overall fold and cofactor arrangement, with a root mean square deviation of 1.26 Å for 2358 C_α atoms. The major differences between the two enzymes concern residues involved in the mechanism of XDH to XO interconversion and crucial residues located within the protein active site. On one hand, lack of residues leading to a flexible loop around the FAD site might explain the fact that AOXs are pure oxidases and do not use NAD⁺ as the final acceptor of reducing equivalents. On the other hand, conserved amino acid residues in each enzyme at the active site are different and may explain the large differ-

ences in substrate and inhibitor specificity between mAOX3 and bXOR. In fact, similar to all the other mammalian AOXs, mAOX3 oxidizes a different set of substrates in comparison to XORs.

XDH/XO Interconversion Domain—The reversible XDH to XO interconversion involves the formation of a new disulfide bond between two cysteine residues (Cys-535 and Cys-992) that are not conserved in mAOX3 being substituted by Tyr-542 and Phe-997, respectively. Both reversible and irreversible interconversion of XDH into XO requires structural rearrangement of an 11-residue loop, referred to as the “variable loop” (Gln-423–Lys-433 in bovine XOR), which is in close proximity to the FAD cofactor. The amino acid sequences of the loop are rather divergent in mAOX3 and bXOR (Fig. 4). The loop movement leads to a change in the electrostatic environment around the FAD cofactor influencing its redox potential (which changes from −410 mV in XDH to −234 mV in XO (30)). In XO, the loop position blocks access of NAD⁺ to its binding site near FAD. As a consequence, the XO form does not bind NAD⁺ and uses oxygen as the final electron acceptor instead. In mAOX3 the final electron acceptor is always oxygen, and we anticipated that the structure of the corresponding variable loop would be similar to the one observed in the XO form of XOR. In fact, the FAD cofactor exhibits similar redox potentials in XO (−234 mV) and rabbit AOX (−212 mV) (30, 33).

Surprisingly, the mAOX3 loop turned out to be totally superimposable with the one present in the XDH form (Fig. 5). The 11 residues that comprise the loop are conserved in bovine and human XOR but not in AOXs. Of the 11 residues in the highly charged XOR loop (⁴²³QASRRREDDIAK⁴³³) only 4 are con-

The First Crystal Structure of Mouse Liver Aldehyde Oxidase

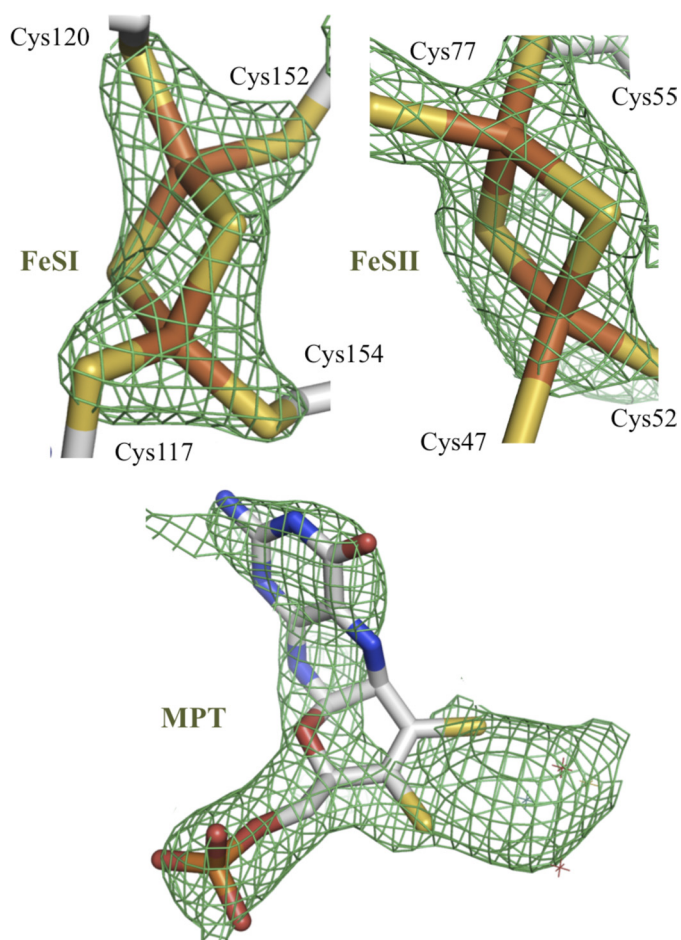


FIGURE 2. Simulated annealing omit electron density map contoured at 1.0 σ and superimposed with the final refined model for [2Fe-2S] I, [2Fe-2S] II and molybdopterin monophosphate cofactor (MPT) (monomer A).

served in mAOX3 (⁴³⁰QAPRQQNAFAT⁴⁴⁰) or human AOX1 (Fig. 5). Interestingly, although 6 of the 11 residues are charged in XOR, only the conserved Arg-433 is charged in AOXs. In addition, XOR Arg-427, which is substituted by Gln-434 in mAOX3, belongs to the cluster of conserved amino acid residues (Arg-335, Trp-336, Arg-427, Phe-549, XOR numbering) responsible for the switching between XO and XDH (31, 34). These residues are also not conserved in *R. capsulatus* XDH, which cannot be converted to the XO form either. Arg-427 corresponds to a Gln in AOXs and to an Asp in *R. capsulatus* XDH. Trp-336 (bXOR numbering) plays a major role in the interconversion mechanism and is substituted by a Thr in AOXs and by an Arg in *R. capsulatus* XDH. All these different structural elements responsible for the XDH to XO conversion are absent in the mouse and human AOXs and are probably related to the inability of an interconversion mechanism by AOX.

Active Site and Substrate Access Funnel—All residues in the active site of mAOX3 have well defined electron density, but the limited resolution of the data (2.9 Å) did not allow unambiguous identification of all molybdenum coordinating ligands. Because these are known to be the same as in XOR, they were defined according to the crystal structure of homologous bXDH (2.0 Å resolution) (35). As in all members of the molybdo-flavoenzyme XOR family, molybdenum adopts a dis-

torted square pyramidal coordination geometry, with the two sulfur atoms from the dithiolene in the equatorial plane (Mo-S distances, 2.4–2.7 Å, values for the 4 molecules in the asymmetric unit). The two other equatorial positions include the catalytically essential sulfur atom (=S) (not clear in the structure because of insufficient resolution) and the equatorial OH group (Fig. 2) that is the source of the transferred oxygen. An oxygen atom (=O) occupies the apical position. When comparing the active site structures of mAOX3 and bXDH (Fig. 6, Table 2), important conserved residues are Gln-772, Glu-1266, Phe-919, and Phe-1014 (mAOX3 numbering). The two conserved Phe residues (Phe-919 and Phe-1014) are responsible for the orientation of substrate and inhibitor molecules in XORs through stacking interactions (36). As in bXOR, Gln-772 makes a hydrogen bond with the apical oxygen ligand, and Glu-1266 is in contact with the hydroxyl ligand. This strictly conserved glutamate has been shown to be crucial for catalysis in XOR enzymes, playing a fundamental and direct role in the reaction mechanism initiating it as an active site base (28). In our studies Glu-1266 was exchanged by a glutamine, and variation of this residue resulted in a complete loss of activity with different *N*-heterocyclic compounds as substrates (Table 3). However, a residual activity with benzaldehyde was obtained (60% reduction of activity in comparison to the wild type enzyme) that might be explained by the higher electrophilicity of the carbonyl carbon atom in aldehydes, as compared with the *N*-heterocyclic compounds, which are substrates of XOR. Other key residues located in the catalytic core are not conserved in AOX3 and XOR and were expected to be responsible for most of the differences in substrate binding, specificity, and catalysis. Of particular relevance are the charged residues Glu-802 and Arg-880 in bXDH that correspond to Ala-807 and Tyr-885 in AOX3, respectively (Fig. 6, Table 2). It was suggested from the XDH crystal structure that Glu-802 and Arg-880 are essential for the correct positioning/orienting and/or activation of the substrate through the establishment of hydrogen bonds and electrostatic interactions (36), as found in all structures of XOR complexed to inhibitors or substrates (29, 37–40). Glu-802 in bXDH is replaced by a valine in all AOX1 orthologs and by an alanine (Ala-807) in mAOX3. This might allow the accommodation of bulkier substrates at the protein active site. In addition, an uncharged residue contributes to the necessary environment for the binding of differently charged compounds. The conserved Arg-880 of bXDH is replaced by methionine in all AOX1 orthologs, a phenylalanine in all mAOX4 and all mAOX311 orthologs, and by a Tyr-885 in mAOX3. As shown in the crystal structure, the aromatic ring of this amino acid points outward from the substrate binding cavity, possibly leading to a further increase in the ability of the mAOX3 active site to accommodate bulkier substrates (Fig. 6). Mutagenesis studies of the two XDH residues (Glu-803 and Arg-881 in human XOR numbering) were performed by Yamaguchi *et al.* (41) in an attempt to alter the substrate specificity from the XOR to the AOX type. Two mutants (E803V, R881M) acquired the ability to oxidize some recognized AOX substrates, whereas their capacity to oxidize hypoxanthine or xanthine was impaired. The authors predicted that the substrate specificity of XOR should change completely to AO by the double mutant E803V/

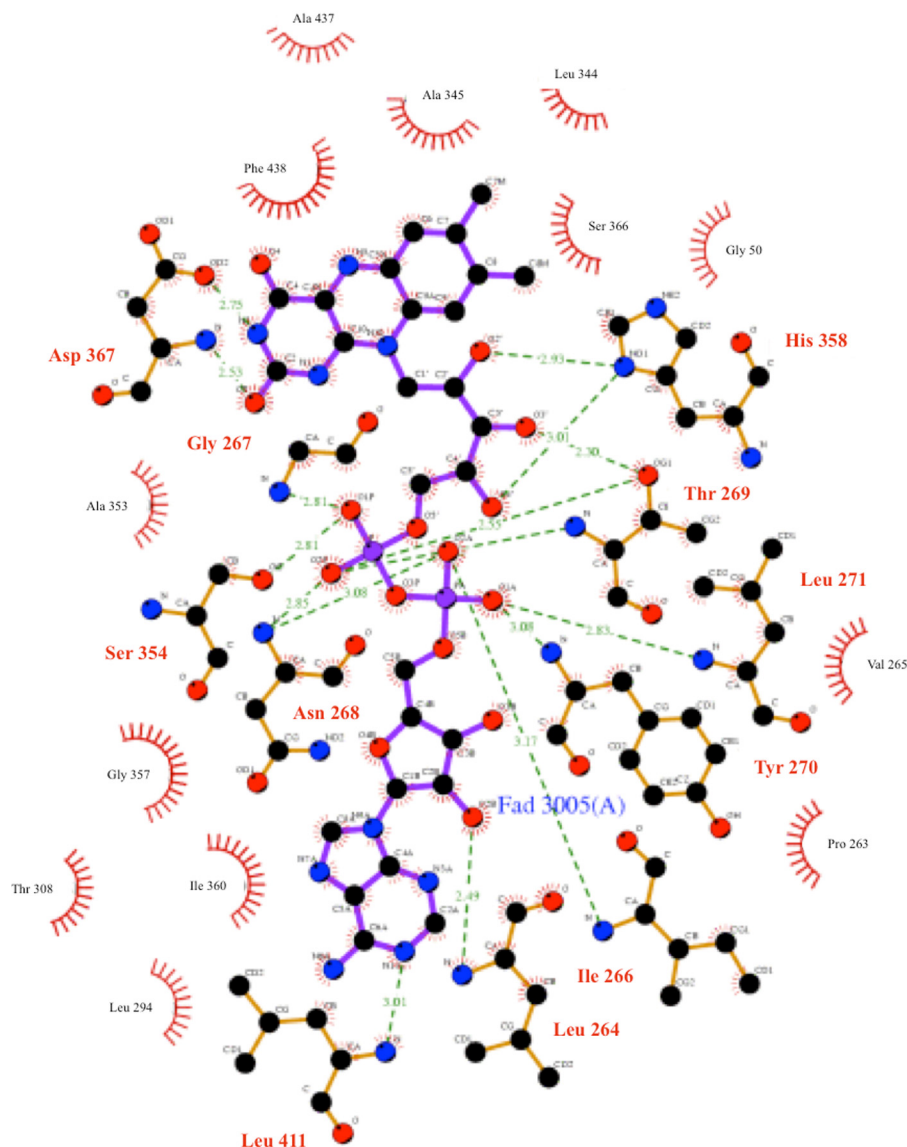


FIGURE 3. **LIGPLOT** representation of mAOX3 environment in the FAD binding site. N and O atoms are represented as blue and red balls, respectively. Ligand bonds are in purple, non-ligand bonds are in light brown and hydrogen bonds are green dashed lines. Non-ligand residues in hydrophobic contacts with the ligand, are presented by red semi-circles with radiating spokes.

R881M, but the latter could not be purified. In contrast, the exchange of these residues in mAOX1 (V804E, M884R, and V804E/M884R) to the ones present in XOR gave no rise in activity with xanthine or hypoxanthine as substrates (42). This finding implicated that more residues in the active center are involved in substrate binding and conversion than the two residues directly involved in substrate binding. To study the influence of these residues in mAOX3 activity, Ala-807 was exchanged to a valine and Tyr-885 to a methionine, the conserved residues in all AOX enzymes. The A807V variant of mAOX3 did not affect the kinetic constants with smaller substrates like benzaldehyde or phthalazine (Table 3). However, the affinity for bulkier substrates like phenanthridine was decreased, whereas the catalytic efficiency was slightly raised. Upon conversion of Tyr-885 to methionine, the kinetic constants also remained mainly the same, with small hydrophobic substrates like benzaldehyde and phthalazine (Table 3). These substrates were converted with unchanged rate constants, and

only a minor increase in K_m was observed, possibly due to the smaller hydrophobic pocket in the Y885M variant. On the other hand, bulkier substrates like phenanthridine or more charged substrates like *N*1-methylnicotinamide were converted with higher efficiency. This may be due to the higher flexibility of the methionine side chain in comparison to tyrosine that may facilitate the binding of these substrates. The effects were much more pronounced in the double variants (Table 3).

Another important charged residue close to the active site of mAOX3 is Lys-889, which is conserved in all AOX enzymes and replaced by His in XORs (His-884). Lys-889 lies ~ 10 Å away from the molybdenum center and ~ 6 Å away from Glu-1266. This lysine adopts a position similar to the conserved Arg-880 of XDH (Fig. 6). Molecular dynamics simulations demonstrated that substrate docking into the active site causes Lys-889 to move from its original position, establishing new interactions with Glu-1266 and/or the substrate itself (supplemental Fig. S1). Lys-889 is located close to the funnel pathway and limits

The First Crystal Structure of Mouse Liver Aldehyde Oxidase

1 20 40 60 80

mAOX3 MGSSHHHHHSSGLVPRGSMSPSKESDELIFVFNKGKVTERNADPEVNLFLYLRKVI RL TGTKYGGGGGCGACTVMISRYDPI SKRISHFSATACLVPI
hAOX1 -----MDRASLELLFYVNGRVI I EKNVDPETLLMPYLRKKLRL TGTPTYGGGGGCGACTVMISRYNP I TRKR RHHPANACL IPI
bXDH -----MTADELVFVFNKGKVKVEKNADPETLL LAYLRKKLRL TGTPTYGGGGGCGACTVMISRYDRLQDK I I HFSANACL API
hXOR -----MTADKLVFVFNNGRVI EKNADPETLL LAYLRKKLRL TGTPTYGGGGGCGACTVMISRYDRLQDK I I HFSANACL API
RcXDH -----MEI AFLNNGTRVRVIEDPTQS LLELRRAEGL TGTKEGCGNEGDCGACTVM I - - - RDAAGSRVNAAGLMM

100 120 140 160 180

mAOX3 CSLHGAAVTVVEGIGSTKTR I HPVQ ERI AKHGCTCGCFCTPGMVM I YTLRNHPPESTEQIMETLGNLCRCCTGYRPIVESAKSFCSSTCCQMNGEGK
hAOX1 CSLHGAAVTVVEGIGSTKTR I HPVQ ERI AKHGCTCGCFCTPGMVM I YTLRNHPPESTEQIMETLGNLCRCCTGYRPIVESAKSFCSSTCCQMNGEGK
bXDH CTLLHVAVTVVEGIGSTKTR I HPVQ ERI AKHGCTCGCFCTPGMVM I YTLRNHPPESTEQIMETLGNLCRCCTGYRPIVESAKSFCSSTCCQMNGEGK
hXOR CSLHVAVTVVEGIGSTKTR I HPVQ ERI AKHGCTCGCFCTPGMVM I YTLRNHPPESTEQIMETLGNLCRCCTGYRPIVESAKSFCSSTCCQMNGEGK
RcXDH PQIAGKALRTI EGI AADPGRI HPVQ ERI AKHGCTCGCFCTPGMVM I YTLRNHPPESTEQIMETLGNLCRCCTGYRPIVESAKSFCSSTCCQMNGEGK

200 220 240 260

mAOX3 CCLDEEKN - - - EPERKNSVCTKLYEKKEFQPLDPTQEL I FPELPMRAAESQNTV LFRGERTTWIAPGTLNDL LELKMKHPSAPLV I GNTYGLGHMKFT
hAOX1 CCLDQGINGLPEFEFGSKTSPKLF AEEFLPLDPTQEL I FPELPMIMADKQSORTVLFRGERTTWIAPGTLNDL LELKMKHPSAPLV I GNTYGLGHMKFT
bXDH NCCMNQKK - - - DHTVLSLPSLFNPEEFPLDPTQEP I FPELPMIMADKQSORTVLFRGERTTWIAPGTLNDL LELKMKHPSAPLV I GNTYGLGHMKFT
hXOR NCCMNQKK - - - DHTVLSLPSLFNPEEFPLDPTQEP I FPELPMIMADKQSORTVLFRGERTTWIAPGTLNDL LELKMKHPSAPLV I GNTYGLGHMKFT
RcXDH FTLAQLSSGV - - - -----RQGTAPAF LPEISDALADWYLAHFEATL I AGCTDVSLWWTKA

280 300 320 340 360

mAOX3 DVSYPI I I SPAR I LELFVVTNKG LTL TGLSLTQVKNVLSDDVSR I PKEKTI YCALLKQ I KTLAGQC I RNVASLGGH I I SRLP TSD LNF I LG I GNC I
hAOX1 GVFHPGYNPDR I EEECPCKP I YCLT LAGLSLAQVK I I LADVVQK I PEEKTQMYHALLKH I GTLAGQC I RNVASLGGH I I SRLP TSD LNF I LG I GNC I
bXDH NQLFP M I CPAWI PELNAVEHPG E I SFAACALSSVEKTL EAVAK I PTKQTEVFRGVLEQ I RWFAGKQ VKSVA SVG GNT I I TASP I SD LNF VFMASGK
hXOR NMLFP M I CPAWI PELNSVEHPG E I SFAACALSSVEKTL EAVAK I PTKQTEVFRGVLEQ I RWFAGKQ VKSVA SVG GNT I I TASP I SD LNF VFMASGK
RcXDH LRLDPEVAFLSHCKDLA Q I RETPDEYGI SAGVT - - - I AARAFAE GPHPALG I RRFASEQVROVA T I GNTANGS I I GGGP AL I AMGAS

380 400 420 440 460

mAOX3 I NVASTEG I QQ I PLNDH I LAGVPDA I LKPEQVLI I SVFVPRS SKWFEVSAFR QAPRQNAFAT I VNAGMKVVFKEEDNT I TDGL I LYGG I GATVI I SAKDSKCR
hAOX1 I NLLSKEGKRQ I PLNEO I LSKCPNADLKPEI I LVSNIPI I SRKWFVEVSAFR QARQENAL I VNSGMRVFFEGGDG I I RELC I SYGGVGRPI I CAKNSCQ
bXDH I TIVSRGTRRTVMDHT I FFGYKTL LGPEE I LLS I E I PYSREFFSAF QASRREDD I AKVTSGMRVL FQPGSMQVLEK I I TASP I SD LNF VFMASGK
hXOR I TILVSRGTRRTVMDHT I FFGYKTL LGPEE I LLS I E I PYSREFFSAF QASRREDD I AKVTSGMRVL FQPGSMQVLEK I I TASP I SD LNF VFMASGK
RcXDH I TLRGQERRRMPLEDF I LEYRKQDRRPFGEFVS VTLPKSAPGLRCYKLSKRFDDQ I SAVGCC - - - LNLTLKGSKI ETAR I AFGGMAGVPKRAAFAEA

480 500 520 540 560

mAOX3 QLI GRWD I EMLD DDAKMI I CEVSL LMAAPGGMEYRKT I A I SFLFMFYLDV LKQL - KTRDPHKYPD I SQKLL I LEDF LPTMPYGMQS FQDVFQPLQ
hAOX1 KLI GRWH I EMLD I ACLRI I LNELSL LGSAPGGVEFKRT I I I SFLFKFYLDV LKQL - KMDPVHYPKSLADKYESAL EDLHSHKSTLKYQNI I GPKHPE
bXDH KQLSKFWN I KLDQV CAGLA EELS LSPDAPGGMI I EFRRTL T L S FFFKYLTV LKLGKDS - KDKCGKLDPTYTAS L L FQKDPAN I QLFQEVNPKQSKE
hXOR KQLSKFWN I KLDQV CAGLA EELS LSPDAPGGMI I EFRRTL T L S FFFKYLTV LKLGKDS - KDKCGKLDPTYTAS L L FQKDPAN I QLFQEVNPKQSKE
RcXDH AL I GQDFR I EDT I AALP L LAQDFT L L S D M - - - -----RASAAYRMNAQAQALRYVRELSGEAVAVLEVMP

580 600 620 640 660

mAOX3 DP I GR I IM I QSG I KHAT I EA I V F CDD I MSVLPGE I I LAVVTSSKSHAK I I I SLDASEALASL CVVDVVTAR DVPDGD I GREE - - - I SLYAODEV I CVGQ I VCA
hAOX1 DP I GR I IM I LSGV KHAT I EA I Y CDD I MPLVDQE I I I T V T SRAHAK I I VNSD I SEALSMPGVVD I IMTAEHLSDVNSFCFTEAK I I ADTKVFCVGH I VCA
bXDH DTVGRRLP I LAAMAQAS I EA I V Y CDD I I PRYENEL I RLVTS I TRAHAK I I KS I D I SEAKV P F V C F I S A D D V G S I I T G I C N D - I T V F A K D K V T C V G H I I G A
hXOR DMVGRRLP I LAAMAQAS I EA I V Y CDD I I PRYENEL I RLVTS I TRAHAK I I KS I D I SEAKV P F V C F I S A D D V G S I I T G I C N D - I T V F A K D K V T C V G H I I G A
RcXDH MSVCKLP I L D SARAHTV I QARYLD I LCPANT I H I A F G L S T E A S A A I T G L D L E P V R E S P E V I A V F T A D L P H D N A S P A S P E P V L A T G E V H F V G P I I F L

680 700 720 740 760

mAOX3 V A A D S Y A H A Q A A K K V K I V Y Q D I E P M I V T V Q D A L Q Y E S F I G P E R K L E Q N V E E A F Q C A D Q I L E G E V H L G G E H F Y L E T Q S R V R V P K G E D K E M D I Y V S S O D
hAOX1 V L A D S E V Q A K R A A K R V K I V Y Q D L E P L I T I E E S I Q H N S S F K P E R K L E Y N D V E A F K V V D Q I L E G E I H M G G E H F Y L E T Q S M L V P K G E D E M V D Y S T O F
bXDH V V A D T P E H A E R A A H V V K V T Y E D L - P A I T I E D A I K N N S F Y G E L K I E K G D L K K G F S E A D N N V S G E L Y I G G G E H F Y L E T H C T I A I P G G E E M E L F V S T O N
hXOR V V A D T P E H A E R A A G V K I T Y E E L - P A I T I E D A I K N N S F Y G E L K I E K G D L K K G F S E A D N N V S G E I Y I G G G E H F Y L E T H C T I A V P K G E A G E M L F V S T O N
RcXDH V A A T S H R A A R I A A R K A R I T Y A R P A I L T L D Q A L A A D S R F E G G P V I W A R G D V E T A L A G A A H L A E C F E I G G G E H F Y L E G Q A A L A L P A - E G G V I H C S S O H

780 800 820 840 860

mAOX3 A A F T E M V A R T L G I P K N R I N C H V R I V G G A F G G K A S K P G L L A S V A A V A A K T G R P I R F I L E R R D M L I T G R R H P L L G K Y I G F M N N K I K A A D I Q L Y I N G G
hAOX1 P K Y I O D I V A S T L K L P A N K V M C H V R I V G G A F G G K V L K T G I I A A V T A F A A N K H R A V R C V L E R G E D M L I T G R R H P Y L G K Y K A G F M N N D R I L A L D M E H Y S N A G
bXDH A M K T O S F V A K M L G V P V N R I L V R V K M G G G F G G E T R S T L S V A V A L A A Y K T G R P V C M L D R N E D M L I T G R R H P F L A R Y K V G F M K T E I V A L E V D H S N A G
hXOR T M K T O S F V A K M L G V P A N R I L V R V K M G G G F G G E T R S T V S V A L A A Y K T G R P V C M L D R N E D M L I T G R R H P F L A R Y K V G F M K T E I V A L E V D H S N A G
RcXDH P S E I C H K V A H A L G L A F H D V R V E M R I C G G F G G K S Q G N H L A I A C A V A A R A T R P C K M R Y D R D D V V I T C K R D F R I R Y R I G A D A S C K L L G A D F V H L A R C E

880 900 920 940 960

mAOX3 C T P D S E L V I E Y A L L K L E N A Y K I P N L R V R G R V C K I N L P S N T A F R G F G F P G A F V T I T C M S A V A A K R L P P E K V R E L N M Y - - - - - R
hAOX1 A S L D E S L F V I E M G L L K M D N A Y K F P N L R C R G W A C R I N L P S N T A F R G F G F P G A V L I T E S C I T E V A A K C G L S P E K V R I I N M Y - - - - - K
bXDH N S R D L S H S I M E R A L F H M D N C Y K I P N I R G T G R L C K I N L P S N T A F R G F G G P Q A L I A E C M S E V A V T C G L P A E E V R K N M Y - - - - - K
hXOR N T O D L S O S I M E R A L F H M D N C Y K I P N I R G T G R L C K I N L P S N T A F R G F G G P Q M L I A E C M S E V A V T C G M P A E E V R K N M Y - - - - - K
RcXDH W S A D L S L P V C R A M L H A D G S V E V P A L R I E S H R L R T N Q S N T A F R G F G G P O G A L G M R A I E H L A R G M G R D P A E L R A L N F Y D P P E R G G L S A P P S P P E P I A T K

980 1000 1020 1040

mAOX3 T I D R T I H N C E F D P T N L L Q C W E A C V E N S S Y N R K K A V D E F T Q O R F W K K R G I A I I P M K F S V G F P K T F Y Y Q A A L V Q I Y T D G S V L V A H G G V E L G G G I N T K Y I O
hAOX1 E I D O T P Y K C E I N A K N L I Q C W R E C M A M S S Y S L R K V A V E K F A E N Y W K K G L A M V P L K F P V G L A S R A A G Q A A L V H I Y L D G S V L V T H G G I E V G O G V H T K Y I O
bXDH E G D L T H F N Q R L E G F S V P R W D E C L K S S Q Y A R K S E V D K F K E N C W K K R G L C I I P T K F G I S F T V P F L N Q A G A L I H V Y T D G S V L V S H G G E T E G O G L H T K Y I O
hXOR E G D L T H F N Q R L E G F L P R C W E E C L A S S Q Y A R K S E V D K F K E N C W K K R G L C I I P T K F G I S F T V P F L N Q A G A L L H V Y T D G S V L L T H G G E T E G O G L H T K Y I O
RcXDH K T Q T H Y G E V A D C V L G E L V T R L Q K S A N F T T R A E I A A W S T N R T L A R G I A L S P V K F G I S E T L T H L N Q A G A L V Q I Y T D G S V L N H G G E T E G O G L H A K V Q

1060 1080 1100 1120

mAOX3 V A S R E L K I P M S Y I H L D E M S T V T V P N T V T T G A S T G A D V N G R A V Q N A C Q I L M K R L E P I I K - - - - - Q N P S G T W E E W K E A F V Q S I L S A
hAOX1 V V S R E R M P M S N V H L R G T S T E T V P N A N I S G G S V A D L N G L A V K P A C Q T L L K R L E P I I S - - - - - K N P K G T W K D W A Q T A F D E S I N L S A
bXDH V A S K A K I P I S K I Y I S E T S I N T V P N S S P T A A S V S T D Y G G A V Y A A G O T I L K R L E P F K K - - - - - K N P D G S W E D W M A A Y Q D R V S L S T
hXOR V A S R A K I P T S K I Y I S E T S I N T V P N T A A S V S A D L N G O A V Y A A G O T I L K R L E P F K K - - - - - K N P S G S W E D W T A A Y M D T V S L S A
RcXDH V A A V A L G I D P V Q V R I T A D D I S K V P N T A T A A S S G A D M N G M A V K D A C E T L R G L A G F V A A R E G C A A R D V I F D A G Q V Q A S G K S W R F A E I V A A Y M A R I S L S A

1140 1160 1180 1200 1220

mAOX3 T C Y F R G Y Q A D M D W E K G E D I P P Y F V F G A A C S E V E I D C L T G A H K N I R T D I V M D V G S F I N P A V D I G Q I E G A F V G G L G L Y T I L E E L K Y S P E G V I Y T R G P H O Y K I
hAOX1 V C Y F R G Y E S D M W E K G E Q P P E Y F V Y G A A C S E V E I D C L T G D H K N I R T D I V M D V G C S I N P A I D I G Q I E G A F I O G M G L Y I I E E L N Y S P Q G I L H T R G P D O Y K I
bXDH T C F Y R T P N L G Y S F E T N S G N P H Y F T Y G V A C S E V E I D C L T G D H K N L R T D I V M D V G S L N P A I D I G O V E G A F V O G L E L F I L E E L H Y S P E G S L H T R G P S T Y K I
hXOR T C F Y R T P N L G Y S F E T N S G N P H Y F Y G V A C S E V E I D C L T G D H K N L R T D I V M D V G S L N P A I D I G O V E G A F V O G L E L F I L E E L H Y S P E G S L H T R G P S T Y K I
RcXDH T C F Y A T P K L S W D R L R G Q R P E L Y F A Y G A I T E V V I D R L T G E N R I L R T D I L H D A G A S L N P A L D I G Q I E G A Y V G A G W L T I E E L W M D H C R L M T H A P S T Y K I

1240 1260 1280 1300 1320

mAOX3 A S V T D I P E E F H V S L L T P T P N P K A I Y S S K G L G A G T F L G C S V F F A I A A A V A A R E E R - - - G L S P I W A I N S P A T A E V I R M A C E D O F T N L V P Q T D S K C K P W S
hAOX1 P A I C D M T E L H I A L L P P S Q N S N T L Y S S K G L G S G V F L G C S V F F A I H D A V S A A R Q E R - - - G L H G P L T L N S P L T P E K I R M A C E D K F T K M I P R D G E S Y V P W N
bXDH P A F G S I Q I E F R V S L L R D C P N K K A I Y A S K A V G P P L F L A A S I F A I K D A I R A R A Q H T G N N V K E L F R L D S P A T P E K I R N A C V D K F T T L C V T G P A G N C K P W S
hXOR P A F G S I Q I E F R V S L L R D C P N K K A I Y A S K A V G P P L F L A A S I F A I K D A I R A R A Q H T G N N V K E L F R L D S P A T P E K I R N A C V D K F T T L C V T G P A G N C K P W S
RcXDH P A F S D R I R I N V A L W D Q P N R E E T I F R S K A V G P P L F L G I S A F L A L H D A C A A C G P H W P D L Q A P A T P E A V L A A V R G A E G R A - - - - -

mAOX3 I P V A
hAOX1 V P I -
bXDH L R V -
hXOR V R V -
RcXDH - - - -

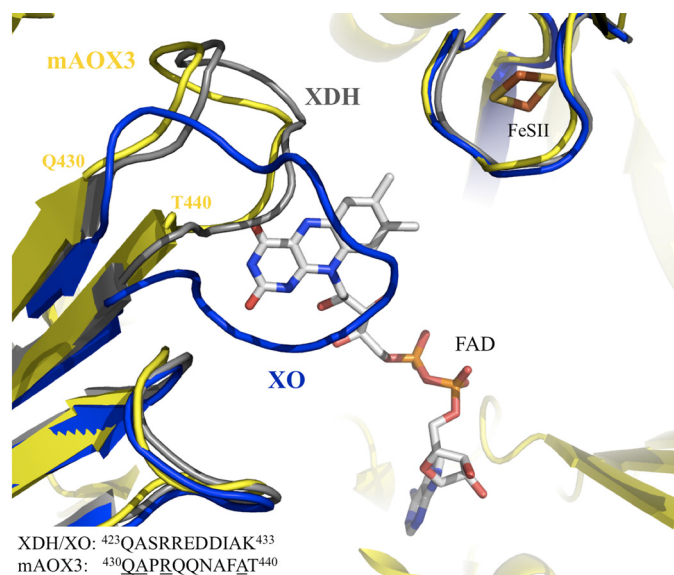


FIGURE 5. Superposition of mAOX3 (yellow), bXDH (gray), and bXO (blue) at the FAD binding site, viewed from the solvent. The FAD and the [2Fe-2S] II are represented color-coded and correspond to the mAOX3 structure. Note the change in the variable loop (residues Gln-423–Lys-433 in bovine XDH numbering) between XO and XDH forms. The FAD molecule occupies a vast area within the protein, with the isoalloxazine ring in close proximity to the solvent-accessible area, and pointing toward the FeII center. The FAD cofactor is 9.0 Å away from the FeII, whereas the distance from the exocyclic NH₂ of the pterin to the nearest FeII is 5.1 Å.

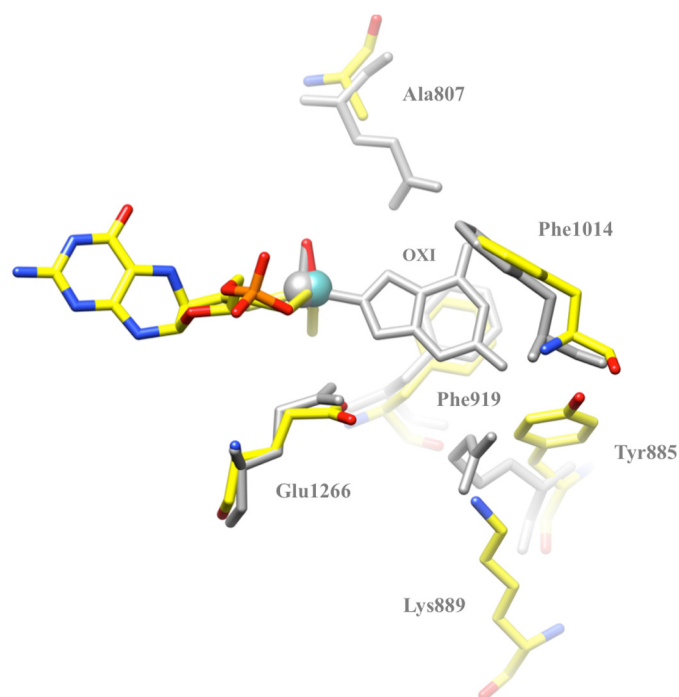


FIGURE 6. Active site comparison between mAOX3 (yellow) and bovine XDH (gray). Outlined are the most important non-conserved residues (mAOX3 numbering). Also present are the XDH inhibitor oxipurinol (OXI) and the conserved XDH and mAOX3 residues Phe-919, Phe-1014, and Glu-1266.

FIGURE 4. Comparison of the amino acid sequences of mouse AOX3, human AOX1, bovine XDH, human XOR, and *R. capsulatus* XDH. The mAOX3 [2Fe-2S] I and II binding Cys residues are marked as (+) and (*), respectively. The conserved (Q772, F919, F1014, E1266) and non-conserved (A807, Y885, K889, P1015) active site residues are marked in gray. Residues R217, D878, L881, and T1081 (in gray) correspond to the substrate access channel. The “variable loop” of the FAD domain (residues Q430–T440) is marked in a box. Black boxes indicate identical residues, and gray boxes, similar residues. (Alignment was created with CLC Sequence viewer Rev 6.5.4.)

the access of larger substrates to the protein active site. Our results show that changing Lys-889 into a histidine leads to a 2–3-fold decrease in the catalytic efficiency using benzaldehyde and phthalazine as substrates, whereas the K_m values remained the same (Table 3). This can be explained by the impaired interaction of His-889 with the substrate (supplemental Fig. S2). Consequently, the nucleophilic attack of the Mo-OH moiety or the stabilization of the transition state is affected. This explanation is in agreement with the finding that the conversion rate constant of phenanthridine is not affected as it does not interact with Lys-889 via an oxygen or nitrogen. Additionally, it is concluded that bulkier substrates or substrates unable to interact with Lys-889 via an oxygen or nitrogen (such as phenanthridine or *N*1-methylnicotinamide, Table 3) also show a lower K_m value in the histidine variant based on its slightly smaller side chain. Structural features along the substrate funnel may also account for the differences in substrate specificities between mAOX3 and XOR. In AOX3 the funnel is ~20 Å wide at the surface and becomes tighter toward the molybdenum catalytic center, where it is ~8 Å wide (Fig. 7). Several residues along the funnel are divergent in the two proteins; particularly, Arg-717, Asp-878, Glu-880, Leu-881, and Thr-1081 of AOX3 are replaced by Leu-712, Leu-873, His-875, Ser-876, and Pro-1076 in XOR (Table 2). Comparison of mAOX3 and bXDH molecular surfaces indicates that the shape and width of the substrate access funnel is more anionic and wider in the case of mAOX3 (Fig. 7). Taken together our results are consistent with the entrance of larger and bulkier substrates for AOXs enzymes in contrast to XORs.

Inhibition by Benzamidine, Menadione, Norharmane, and Raloxifene—Inhibition studies of mAOX3 with raloxifene revealed a mixed type inhibition with calculated inhibition parameters of $K_{ic} = 12.2 \pm 1.8 \mu\text{M}$ and $K_{iu} = 59.1 \pm 5.4 \mu\text{M}$ (Table 4) (43). The inhibition mechanism is in agreement with the two binding modes found in molecular docking studies (see below and the supplemental material, Fig. S3). The higher rigidity of the complex in binding mode (A) can be explained by a stronger interaction, giving rise to a 5-fold lower competitive constant K_{ii} in comparison to K_{ic} . The inhibition constants obtained with purified mAOX3 are 5 orders of magnitude higher than the value previously reported with human liver cytosol (44). The strong inhibition in liver extracts might imply that a more effective raloxifene metabolite is generated in the liver. In contrast, inhibition studies of purified mAOX3 with menadione showed an uncompetitive inhibition with a $K_{ic} = 1.25 \pm 0.04 \mu\text{M}$ (Table 4). This value is comparable to studies by Barr and Jones (45) using human liver lysates, who determined a mixed-type inhibition with $K_{ic} = 0.75 \pm 0.18 \mu\text{M}$ and $K_{iu} = 0.12 \pm 0.0 \mu\text{M}$. The difference in the inhibition mechanism might be explained by the fact that we used DCPIP instead of oxygen as the terminal electron acceptor, and DCPIP was shown to act as an inhibitor itself. Thus, the enzyme-DCPIP

The First Crystal Structure of Mouse Liver Aldehyde Oxidase

TABLE 2

Comparison of relevant residues (conserved and non-conserved) of mAOX3 (and hAOX1) (blue) and bovine XDH (green) present in the substrate binding pocket and in the substrate access channel

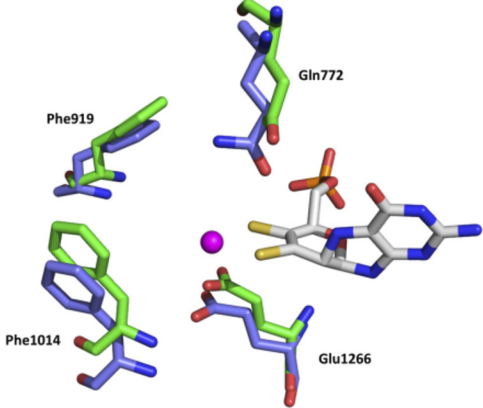
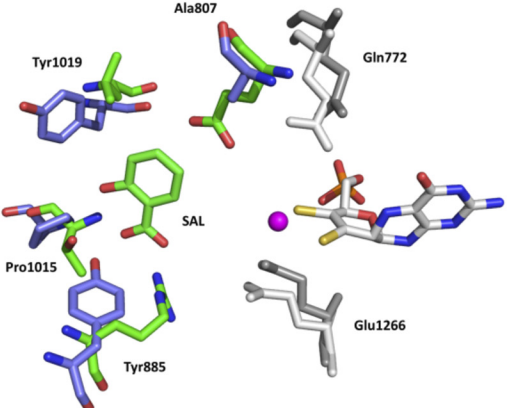
Residues	Location	mAOX3 (hAOX1)	bXDH
Conserved	 <p>Active site</p>	Gln772 (Gln)	Gln767
		Phe919 (Phe)	Phe914
		Phe1014 (Leu)	Phe1009
		Glu1266 (Glu)	Glu1261
Non-conserved	 <p>Active Site</p>	Ala807* (Val)	Glu802
		Tyr885* (Met)	Arg880
		Lys889* (Lys)	His884
		Pro1015 (Gly)	Thr1010
		Tyr1019 (Ala)	Leu1014
	Substrate Access Chanel	Arg717 (Arg)	Leu712
		Asp878 (Glu)	Leu873
		Glu880 (Leu)	His875
		Leu881 (Phe)	Ser876
		Thr1081 (Ile)	Pro1076

TABLE 3

Kinetic parameters of mAOX3 variants obtained at 37 °C, pH 8.00

ND, none detectable.

Substrate	Benzaldehyde ^a			N1-Methylnicotinamid ^a		
	k_{cat} min^{-1}	K_m μM	k_{cat}/K_m $\mu\text{M}/\text{min}$	k_{cat}^b min^{-1}	K_m μM	k_{cat}/K_m $\mu\text{M}/\text{min}$
mAOX3-WT	41.9 ± 0.8	2.5 ± 0.2	16.76	14.7 ± 0.1	128.5 ± 5.8	0.115
E1266Q	10.2 ± 0.5	86.3 ± 11.3	0.12	ND	ND	
A807V	41.0 ± 0.3	2.9 ± 0.2	14.14	11.2 ± 0.1	123.4 ± 5.4	0.091
Y885M	57.4 ± 0.8	6.3 ± 0.3	9.11	23.4 ± 0.4	82.7 ± 6.6	0.283
A807V/Y885M	43.6 ± 1.1	4.6 ± 0.4	9.48	27.0 ± 0.2	35.9 ± 1.4	0.752
K889H	19.2 ± 0.5	2.3 ± 0.3	8.20	3.1 ± 0.1	25.5 ± 4.0	0.120

Substrate	Phenanthridine ^b			Phthalazine ^a		
	k_{cat} min^{-1}	K_m μM	k_{cat}/K_m $\mu\text{M}/\text{min}$	k_{cat} min^{-1}	K_m μM	k_{cat}/K_m $\mu\text{M}/\text{min}$
mAOX3-WT	51.7 ± 0.6	32.3 ± 1.4	1.60	41.1 ± 1.0	1.4 ± 0.2	29.36
E1266Q	ND	ND		ND	ND	
A807V	315.0 ± 5.2	149.5 ± 5.8	2.11	41.1 ± 1.5	2.7 ± 0.4	15.22
Y885M	266.9 ± 66.5	33.4 ± 11.6	7.99	48.9 ± 1.2	3.2 ± 0.2	15.28
A807V/Y885M	218.0 ± 17.1	11.8 ± 1.7	18.47	41.4 ± 1.8	2.9 ± 0.3	14.28
K889H	79.9 ± 0.7	16.1 ± 0.6	4.97	11.8 ± 0.3	1.1 ± 0.2	10.53

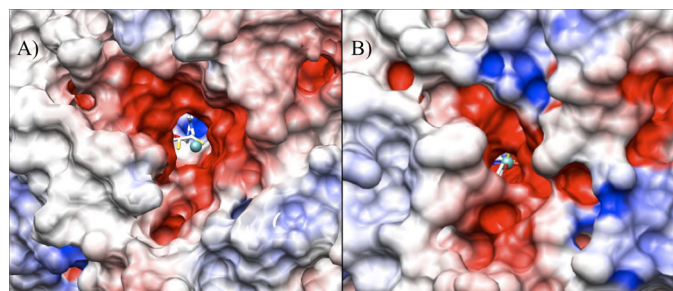
^a As terminal electron acceptor 100 μM DCPIP were used.^b As terminal electron acceptor molecular oxygen in air saturated buffer was used.

FIGURE 7. Surface representation of the funnel leading to the active site in mAOX3 (A) and bovine XDH (B). The molybdenum atom is seen at the end of the funnel as a green sphere. The entrance is much wider in the case of mAOX3, with a narrow constriction closer to the molybdenum active site. Electrostatic surface potentials were calculated using the Delphi program and are represented in PyMol (52) (surface potential color from -0.10 V, negatively charged in red, to $+0.10$ V, positively charged in blue).

TABLE 4

Kinetic parameters of phthalazine-DCPIP reaction in the absence or presence of benzamidine, menadione, norharmine, and raloxifene obtained at 37 °C pH 8.00

Only the appropriate inhibition parameters (K_{ic} represents the competitive constant, and K_{iu} represents the uncompetitive constant) were included in the fit to Equation 1.

	k_{cat}	K_m	K_{ic}	K_{iu}
	min^{-1}	μM	μM	μM
Benzamidine	40.7 ± 0.3	1.3 ± 0.0	22.5 ± 0.8	—
Menadione	38.6 ± 0.4	1.6 ± 0.1	—	1.25 ± 0.04
Norharmine	49.0 ± 0.6	2.0 ± 0.1	0.18 ± 0.01	—
Raloxifene	43.7 ± 0.8	1.8 ± 0.1	12.2 ± 1.8	59.1 ± 5.4

complex might prevent menadione binding in a competitive manner. Benzamidine was shown to be a competitive inhibitor of rat and bovine XO (46) with K_{ic} values of 30 and 3 mM, respectively. Benzamidine inhibited native rat AOX and mAOX3 at similar millimolar concentrations (47, 48). An estimated K_{ic} of 25 μM can be calculated from the data of Vila *et al.* (47) using a competitive Michaelis-Menten model. Our data agree with these results and show a competitive inhibition with a $K_{\text{ic}} = 22.5 \pm 0.8 \mu\text{M}$ (Table 4). Norharmine was shown to inhibit the 2-OH-pyrimidine:ferricyanide reaction of native

mAOX3 in a non-competitive manner with $K_{\text{ic}} = 0.68 \mu\text{M}$ (47). Our data show a competitive inhibition with a $K_{\text{ic}} = 0.18 \pm 0.01 \mu\text{M}$ (Table 4). The differences between the two inhibition modes are explained by the use of ferricyanide as final electron acceptor in the former study, which does not interfere with the molybdenum site, whereas DCPIP interacts with the molybdenum site (49). In conclusion, raloxifene shows a different behavior in human liver lysate and purified mAOX3, showing a possible metabolism of raloxifene in the liver, which results in a more effective inhibitor.

Molecular docking studies using raloxifene identified two different binding modes. In mode (A) (Fig. 8A) it is one of the phenol moieties that enters into the pocket, whereas in mode (B), it is the piperidyl group that takes its place (Fig. 8B). For this reason, we performed molecular dynamics studies on the two raloxifene binding modes. As expected, in mode (A), when the inhibitor enters the active site via the phenol, there is less variation in its position. Raloxifene interacts with the pocket via a hydrogen bond with Glu-1266 and aromatic stacking interaction with Phe-919. In mode (B) there is only a van der Waals interaction between the piperidyl group of the inhibitor and Phe-919 in the Moco pocket.

Reaction Mechanism—The presence of some highly conserved residues at the catalytic center (Glu-1266, Phe-919, Gln-772 in mAOX3 numbering) as well as the type of reaction catalyzed suggests that the reaction mechanism for both AOXs and XORs is similar, although not identical, as AOXs exhibit much broader substrate specificity. The reaction mechanism that we propose for AOXs with the substrate phthalazine is illustrated in Fig. 9. The reaction starts by the nucleophilic attack of the activated Mo-OH ligand (activated by Glu-1266) on the carbon atom of the substrate (carbon atom adjacent to an aromatic nitrogen atom) (Fig. 9, *step i*). Concomitantly, hydride transfer occurs to the sulfido ligand, and an intermediate species is formed. This intermediate is stabilized by hydrogen bonding interactions with residues of the active site, namely Glu-1266 and Lys-889. This concerted mechanism is

The First Crystal Structure of Mouse Liver Aldehyde Oxidase

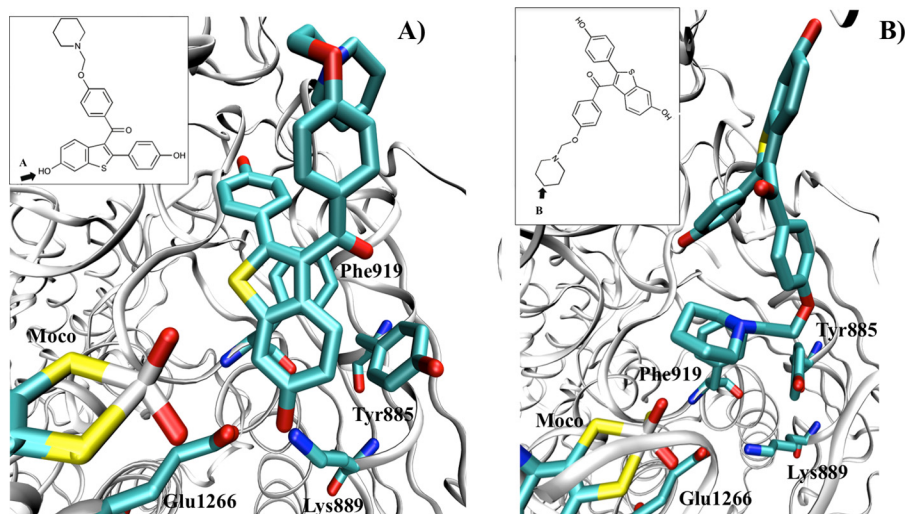


FIGURE 8. Molecular docking studies with the inhibitor raloxifene; binding modes (A) and (B).

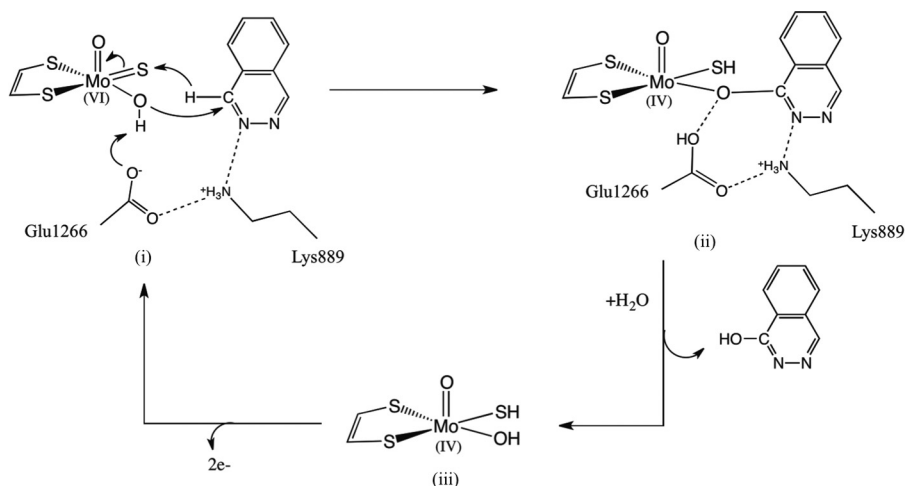


FIGURE 9. General reaction mechanism for aldehyde oxidases exemplified for the substrate phthalazine (mAOX3 residue number).

avored by experimental evidence with substituted *N*-heterocycles as well as by recent density functional theory calculations (50). In *step ii*, the product is released from the reduced molybdenum site, and a water molecule replenishes the vacant coordination position. The reaction cycle is closed (*step iii*) once molybdenum is re-oxidized, and the two reducing equivalents are transferred to molecular oxygen via the two [2Fe-2S] clusters and the FAD cofactor. It is expected that the proton transfer from the hydroxyl ligand of molybdenum to Glu-1266 disrupts the interaction of Glu-1266 with Lys-889. This forces Lys-889 to move away from Glu-1266 and the molybdenum center, where it can interact with the product before the latter is released from the active site.

Conclusions—The present crystal structure constitutes the first of an aldehyde oxidase protein, having major importance to clarify its substrate specificity. When compared with XORs, the broader range of substrates as well as the kinetic behavior of AOXs can now be explained. The mAOX3 overall structure is similar to XORs but shows marked differences around the FAD. Detailed analysis of the protein active center in addition to docking and simulation studies have shown that the different substrate specificities between AOXs and XORs are related to

the non-conservation of several protein residues, not only in the active site as expected, but also in the active site funnel pathway. Docking studies on the mAOX3 structure enabled the revealing of specific inhibitor interactions. For the highly potent human AOX1 inhibitor raloxifene, two binding modes were predicted by the computational studies, in agreement with our kinetic data. However, a different inhibition mechanism was found in purified mAOX3 in comparison to previous studies in whole-cell lysates. Site-directed mutagenesis of mAOX3 combined with molecular docking studies for several types of substrates revealed new protein-substrate interactions, highlighting the role of the highly conserved Lys-889 in substrate binding and its putative involvement in the reaction mechanism of aldehyde oxidases.

Acknowledgments—We thank the ID14-1 and ID23-2 staff of the ESRF (Grenoble, France) for assistance during data collection.

REFERENCES

- Garattini, E., Fratelli, M., and Terao, M. (2008) Mammalian aldehyde oxidases. Genetics, evolution, and biochemistry. *Cell. Mol. Life Sci.* **65**, 1019–1048

2. Garattini, E., Fratelli, M., and Terao, M. (2009) The mammalian aldehyde oxidase gene family. *Hum. Genomics* **4**, 119–130
3. Garattini, E., Mendel, R., Romão, M. J., Wright, R., and Terao, M. (2003) Mammalian molybdo-flavoenzymes, an expanding family of proteins. Structure, genetics, regulation, function, and pathophysiology. *Biochem. J.* **372**, 15–32
4. Terao, M., Kurosaki, M., Saltini, G., Demontis, S., Marini, M., Salmons, M., and Garattini, E. (2000) Cloning of the cDNAs coding for two novel molybdo-flavoproteins showing high similarity with aldehyde oxidase and xanthine oxidoreductase. *J. Biol. Chem.* **275**, 30690–30700
5. Terao, M., Kurosaki, M., Marini, M., Vanoni, M. A., Saltini, G., Bonetto, V., Bastone, A., Federico, C., Saccone, S., Fanelli, R., Salmons, M., and Garattini, E. (2001) Purification of the aldehyde oxidase homolog 1 (AOH1) protein and cloning of the AOH1 and aldehyde oxidase homolog 2 (AOH2) genes. Identification of a novel molybdo-flavoprotein gene cluster on mouse chromosome 1. *J. Biol. Chem.* **276**, 46347–46363
6. Terao, M., Kurosaki, M., Demontis, S., Zanotta, S., and Garattini, E. (1998) Isolation and characterization of the human aldehyde oxidase gene. Conservation of intron/exon boundaries with the xanthine oxidoreductase gene indicates a common origin. *Biochem. J.* **332**, 383–393
7. Terao, M., Kurosaki, M., Barzago, M. M., Varasano, E., Boldetti, A., Bastone, A., Fratelli, M., and Garattini, E. (2006) Avian and canine aldehyde oxidases. Novel insights into the biology and evolution of molybdo-flavoenzymes. *J. Biol. Chem.* **281**, 19748–19761
8. Calzi, M. L., Raviolo, C., Ghibaudi, E., de Gioia, L., Salmons, M., Cazzaniga, G., Kurosaki, M., Terao, M., and Garattini, E. (1995) Purification, cDNA cloning, and tissue distribution of bovine liver aldehyde oxidase. *J. Biol. Chem.* **270**, 31037–31045
9. Rodríguez-Trelles, F., Tarrío, R., and Ayala, F. J. (2003) Convergent neofunctionalization by positive Darwinian selection after ancient recurrent duplications of the xanthine dehydrogenase gene. *Proc. Natl. Acad. Sci. U.S.A.* **100**, 13413–13417
10. Terao, M., Kurosaki, M., Barzago, M. M., Fratelli, M., Bagnati, R., Bastone, A., Giudice, C., Scanziani, E., Mancuso, A., Tiveron, C., and Garattini, E. (2009) Role of the molybdoflavoenzyme aldehyde oxidase homolog 2 in the biosynthesis of retinoic acid. Generation and characterization of a knockout mouse. *Mol. Cell. Biol.* **29**, 357–377
11. Kurosaki, M., Terao, M., Barzago, M. M., Bastone, A., Bernardinello, D., Salmons, M., and Garattini, E. (2004) The aldehyde oxidase gene cluster in mice and rats. Aldehyde oxidase homologue 3, a novel member of the molybdo-flavoenzyme family with selective expression in the olfactory mucosa. *J. Biol. Chem.* **279**, 50482–50498
12. Garattini, E., and Terao, M. (2011) Increasing recognition of the importance of aldehyde oxidase in drug development and discovery. *Drug Metab. Rev.* **43**, 374–386
13. Pryde, D. C., Dalvie, D., Hu, Q., Jones, P., Obach, R. S., and Tran, T. D. (2010) Aldehyde oxidase. An enzyme of emerging importance in drug discovery. *J. Med. Chem.* **53**, 8441–8460
14. Eger, B. T., Okamoto, K., Enroth, C., Sato, M., Nishino, T., and Pai, E. F. (2000) Purification, crystallization, and preliminary X-ray diffraction studies of xanthine dehydrogenase and xanthine oxidase isolated from bovine milk. *Acta Crystallogr. D Biol. Crystallogr.* **56**, 1656–1658
15. Enroth, C., Eger, B. T., Okamoto, K., Nishino, T., Nishino, T., and Pai, E. F. (2000) Crystal structures of bovine milk xanthine dehydrogenase and xanthine oxidase. Structure-based mechanism of conversion. *Proc. Natl. Acad. Sci. U.S.A.* **97**, 10723–10728
16. Okamoto, K., and Nishino, T. (2008) Crystal structures of mammalian Xanthine oxidoreductase bound with various inhibitors: allopurinol, febuxostat and FYX-051. *Journal of Nihon Medical School* **75**, 2–3
17. Mahro, M., Coelho, C., Trincão, J., Rodrigues, D., Terao, M., Garattini, E., Saggi, M., Lenzian, F., Hildebrandt, P., Romão, M. J., and Leimkühler, S. (2011) Characterization and crystallization of mouse aldehyde oxidase 3. From mouse liver to *Escherichia coli* heterologous protein expression. *Drug Metab. Dispos.* **39**, 1939–1945
18. Koiwai, H., Akaba, S., Seo, M., Komano, T., and Koshihara, T. (2000) Functional expression of two *Arabidopsis* aldehyde oxidases in the yeast *Pichia pastoris*. *J. Biochem.* **127**, 659–664
19. Team, R. D. C. (2010) *R: A Language and Environment for Statistical Computing*, Foundation for Statistical Computing, Vienna, Austria
20. Leslie, A. G. W., and Powell, H. R. (2007) Processing diffraction data with Mosflm. *Evolving Methods for Macromolecular Crystallography* **245**, 41–51
21. Kabsch, W. (2010) XDS. *Acta Crystallogr. D Biol. Crystallogr.* **66**, 125–132
22. Collaborative Computational Project, Number 4 (1994) The CCP4 suite. Programs for protein crystallography. *Acta Crystallogr. D Biol. Crystallogr.* **50**, 760–763
23. Cowtan, K. (2010) Recent developments in classical density modification. *Acta Crystallogr. D Biol. Crystallogr.* **66**, 470–478
24. Karplus, P. A., and Diederichs, K. (2012) Linking crystallographic model and data quality. *Science* **336**, 1030–1033
25. Emsley, P., and Cowtan, K. (2004) Coot. Model-building tools for molecular graphics. *Acta Crystallogr. D Biol. Crystallogr.* **60**, 2126–2132
26. Afonine, P. V., Grosse-Kunstleve, R. W., and Adams, P. D. (2005) The phenix refinement framework. *CCP4 Newsletter* **42**
27. Rebelo, J. M., Dias, J. M., Huber, R., Moura, J. J., and Romão, M. J. (2001) Structure refinement of the aldehyde oxidoreductase from *Desulfovibrio gigas* (MOP) at 1.28 Å. *J. Biol. Inorg. Chem.* **6**, 791–800
28. Romão, M. J., Archer, M., Moura, I., Moura, J. J., LeGall, J., Engh, R., Schneider, M., Hof, P., and Huber, R. (1995) Crystal structure of the xanthine oxidase-related aldehyde oxidoreductase from *D. gigas*. *Science* **270**, 1170–1176
29. Truglio, J. J., Theis, K., Leimkühler, S., Rappa, R., Rajagopalan, K. V., and Kisker, C. (2002) Crystal structures of the active and alloxanthine-inhibited forms of xanthine dehydrogenase from *Rhodobacter capsulatus*. *Structure* **10**, 115–125
30. Ishikita, H., Eger, B. T., Okamoto, K., Nishino, T., and Pai, E. F. (2012) Protein conformational gating of enzymatic activity in xanthine oxidoreductase. *J. Am. Chem. Soc.* **134**, 999–1009
31. Kuwabara, Y., Nishino, T., Okamoto, K., Matsumura, T., Eger, B. T., and Pai, E. F. (2003) Unique amino acids cluster for switching from the dehydrogenase to oxidase form of xanthine oxidoreductase. *Proc. Natl. Acad. Sci. U.S.A.* **100**, 8170–8175
32. Nishino, T., Okamoto, K., Kawaguchi, Y., Hori, H., Matsumura, T., Eger, B. T., and Pai, E. F. (2005) Mechanism of the conversion of xanthine dehydrogenase to xanthine oxidase. Identification of the two cysteine disulfide bonds and crystal structure of a non-convertible rat liver xanthine dehydrogenase mutant. *J. Biol. Chem.* **280**, 24888–24894
33. Hille, R. (1996) The mononuclear molybdenum enzymes. *Chem. Rev.* **96**, 2757–2816
34. Nishino, T., Okamoto, K., Eger, B. T., and Pai, E. F. (2008) Mammalian xanthine oxidoreductase. Mechanism of transition from xanthine dehydrogenase to xanthine oxidase. *FEBS J.* **275**, 3278–3289
35. Okamoto, K., Eger, B. T., Nishino, T., and Pai, E. F. (2008) Mechanism of inhibition of xanthine oxidoreductase by allopurinol. Crystal structure of reduced bovine milk xanthine oxidoreductase bound with oxipurinol. *Nucleosides Nucleotides Nucleic Acids* **27**, 888–893
36. Okamoto, K., Kawaguchi, Y., Eger, B. T., Pai, E. F., and Nishino, T. (2010) Crystal structures of urate-bound form of xanthine oxidoreductase. Substrate orientation and structure of the key reaction intermediate. *J. Am. Chem. Soc.* **132**, 17080–17083
37. Cao, H., Pauff, J. M., and Hille, R. (2010) Substrate orientation and catalytic specificity in the action of xanthine oxidase. The sequential hydroxylation of hypoxanthine to uric acid. *J. Biol. Chem.* **285**, 28044–28053
38. Dietzel, U., Kuper, J., Doebbler, J. A., Schulte, A., Truglio, J. J., Leimkühler, S., and Kisker, C. (2009) Mechanism of substrate and inhibitor binding of *Rhodobacter capsulatus* xanthine dehydrogenase. *J. Biol. Chem.* **284**, 8768–8776
39. Okamoto, K., Matsumoto, K., Hille, R., Eger, B. T., Pai, E. F., and Nishino, T. (2004) The crystal structure of xanthine oxidoreductase during catalysis. Implications for reaction mechanism and enzyme inhibition. *Proc. Natl. Acad. Sci. U.S.A.* **101**, 7931–7936
40. Pauff, J. M., Zhang, J., Bell, C. E., and Hille, R. (2008) Substrate orientation in xanthine oxidase. Crystal structure of enzyme in reaction with 2-hydroxy-6-methylpurine. *J. Biol. Chem.* **283**, 4818–4824
41. Yamaguchi, Y., Matsumura, T., Ichida, K., Okamoto, K., and Nishino, T. (2007) Human xanthine oxidase changes its substrate specificity to alde-

The First Crystal Structure of Mouse Liver Aldehyde Oxidase

- hyde oxidase type upon mutation of amino acid residues in the active site. Roles of active site residues in binding and activation of purine substrate. *J. Biochem.* **141**, 513–524
42. Schumann, S., Terao, M., Garattini, E., Saggi, M., Lenzian, F., Hildebrandt, P., and Leimkühler, S. (2009) Site-directed mutagenesis of amino acid residues at the active site of mouse aldehyde oxidase AOX1. *PLoS One* **4**, e5348
 43. Cornish-Bowden, A. (1974) A simple graphical method for determining the inhibition constants of mixed, uncompetitive, and noncompetitive inhibitors. *Biochem. J.* **137**, 143–144
 44. Obach, R. S. (2004) Potent inhibition of human liver aldehyde oxidase by raloxifene. *Drug Metab. Dispos.* **32**, 89–97
 45. Barr, J. T., and Jones, J. P. (2011) Inhibition of human liver aldehyde oxidase. Implications for potential drug-drug interactions. *Drug Metab. Dispos.* **39**, 2381–2386
 46. McManaman, J. L., Shellman, V., Wright, R. M., and Repine, J. E. (1996) Purification of rat liver xanthine oxidase and xanthine dehydrogenase by affinity chromatography on benzamidine-Sepharose. *Arch. Biochem. Biophys.* **332**, 135–141
 47. Vila, R., Kurosaki, M., Barzago, M. M., Kolek, M., Bastone, A., Colombo, L., Salmons, M., Terao, M., and Garattini, E. (2004) Regulation and biochemistry of mouse molybdo-flavoenzymes. The DBA/2 mouse is selectively deficient in the expression of aldehyde oxidase homologues 1 and 2 and represents a unique source for the purification and characterization of aldehyde oxidase. *J. Biol. Chem.* **279**, 8668–8683
 48. Moriwaki, Y., Yamamoto, T., Nasako, Y., Takahashi, S., Suda, M., Hiroishi, K., Hada, T., and Higashino, K. (1993) *In vitro* oxidation of pyrazinamide and allopurinol by rat liver aldehyde oxidase. *Biochem. Pharmacol.* **46**, 975–981
 49. Gurtoo, H. L., and Johns, D. G. (1971) On the interaction of the electron acceptor 2,6-dichlorophenolindophenol with bovine milk xanthine oxidase. *J. Biol. Chem.* **246**, 286–293
 50. Alfaro, J. F., and Jones, J. P. (2008) Studies on the mechanism of aldehyde oxidase and xanthine oxidase. *J. Org. Chem.* **73**, 9469–9472
 51. Schumann, S., Saggi, M., Möller, N., Anker, S. D., Lenzian, F., Hildebrandt, P., and Leimkühler, S. (2008) The mechanism of assembly and cofactor insertion into *Rhodobacter capsulatus* xanthine dehydrogenase. *J. Biol. Chem.* **283**, 16602–16611
 52. The PyMOL Molecular Graphics System, Version 1.2r3pre, Schrödinger, LLC